

M. B. Spitzer and C. J. Keavney  
Spire Corporation  
Bedford, Massachusetts 01730

## ABSTRACT

Recent advances in silicon solar cell processing have led to attainment of conversion efficiency approaching 20%. In this paper we review the basic cell design investigated at Spire and indicate features of greatest importance to achievement of 20% efficiency. We discuss in detail experiments to separately optimize high efficiency design features in test structures and discuss the integration of these features in a high efficiency cell. In this work, ion implantation has been used to achieve optimal concentrations of emitter dopant and junction depth. The optimization reflects the trade-off between high sheet conductivity, necessary for high fill factor, and heavy doping effects, which must be minimized for high open circuit voltage. A second important aspect of our design experiments is the development of a passivation process to minimize front surface recombination velocity. We indicate the manner in which a thin SiO<sub>2</sub> layer may be used for this purpose, without increasing reflection losses, if the antireflection coating is properly designed. We also present details of processing intended to reduce recombination at the contact/Si interface. Data on cell performance (including CZ and ribbon) and analysis of loss mechanisms are presented. We conclude with a discussion of the ultimate performance that may be achievable with this type of processing.

## INTRODUCTION

The attainment of 20% conversion efficiency in flat-plate Si solar cells is presently the goal of the National Photovoltaics Program (1). To this end, we have been conducting research on the ion implanted Si cell. This work recently led to the achievement of conversion efficiency of 18%, and efficiency approaching 20% appears possible in the near future (2,3). In this paper, we review the results to date with emphasis on cell processing aspects, and we indicate the device design and cell processing techniques that appear necessary for achievement of the national goal.

The high efficiency cell process to be discussed is based on the use of high lifetime float zone Si. This material was selected owing to superior minority carrier lifetime over a broad resistivity range. One promising alternative is the use of Czochralski silicon, which will be feasible if modest diffusion length ( $\sim 200\mu\text{m}$ ) can be achieved in low resistivity wafers. Many aspects of the techniques to be presented are applicable to polycrystalline material as well, with conversion efficiency commensurate with the diffusion length in such material. We will report in this paper on the application of some of our processing techniques to sheet materials.

PRECEDING PAGE BLANK NOT FILMED

The junction formation technique to be discussed is based on ion implantation and thermal annealing. As was shown in a recent paper, the ion implantation process allows one to reproducibly adjust the emitter dopant concentration to near optimal values (4). In addition, the thermal anneal process can provide a passivating surface oxide if oxygen is admitted to the gas stream. The versatility of this junction formation technique has made possible rapid progress in emitter design.

In order to gain a better understanding of the loss mechanisms operating in our developmental cells, we have used a solar cell modelling code developed at Brown University by one of the authors (5). The results of the modelling will be provided where appropriate throughout this discussion. The one-dimensional model is described in detail in reference 5, and will only briefly be described here.

The modelling code evaluates the analytic solution of the inhomogeneous diffusion equation which we assume governs minority carrier transport in the quasi-neutral emitter and base of the solar cell. The quasi-neutral regions are assumed to terminate at the space-charge region on one side, and at a minority carrier mirror (characterized by a surface recombination velocity) at the other side. The analytic solution for the sum of the diffusion current and a space-charge region light-generated current is integrated over the solar spectrum to obtain short circuit current ( $J_{SC}$ ), open circuit voltage ( $V_{OC}$ ) and efficiency. In addition, provisions have been made for front surface reflection loss, shadow loss, reflection from a back surface mirror, and light-trapping (6).

The equilibrium minority carrier concentrations are calculated using Fermi statistics. The rigid band approximation is used to calculate the effects of band gap narrowing. Position dependence of doping, mobility, and lifetime are not included in this model and this limits the agreement between calculated and measured spectral response for short wavelengths. Nevertheless, we are able to achieve reasonable agreement with most other measurement data.

In the next section, we discuss the selection and characterization of the silicon used in our work. We follow this with a discussion of emitter design and fabrication, including the importance of surface passivation and ohmic contact design. The results of this work indicate the significance of high base minority carrier lifetime, and we report on new results from an investigation of the effects of cell processing on diffusion length. We conclude with a description of the cell design that we are pursuing for attainment of 20% conversion efficiency.

## SELECTION OF SILICON

It is well known that fabrication of superior silicon cells based on conventional p/n junction designs requires silicon of the highest minority carrier lifetime (7). Development of a particular design and process sequence requires knowledge of the post-process lifetime; such data are of particular importance to the selection of base resistivity. For this reason, we investigated post-process lifetime of a variety of float zone slices.

Back surface field (BSF) cells were fabricated using a simple baseline process (1), from float zone slices obtained from Wacker and elsewhere. No antireflection (AR) coatings were used. Figure 1 replicates diffusion length data obtained by the method of Stokes and Chu (9) from quantum efficiency (QE) measurements of completed cells. The triangular data points indicate Wacker WASO-S slices. The square data points are Czochralski slices. Cell data is indicated in Table I. It can be seen that AM1 conversion efficiency is about 10-11% for the WASO-S material of each resistivity. In order to determine how efficiency might be improved, we examined loss mechanisms in detail. In this way we were able to make significant improvements to the baseline process.

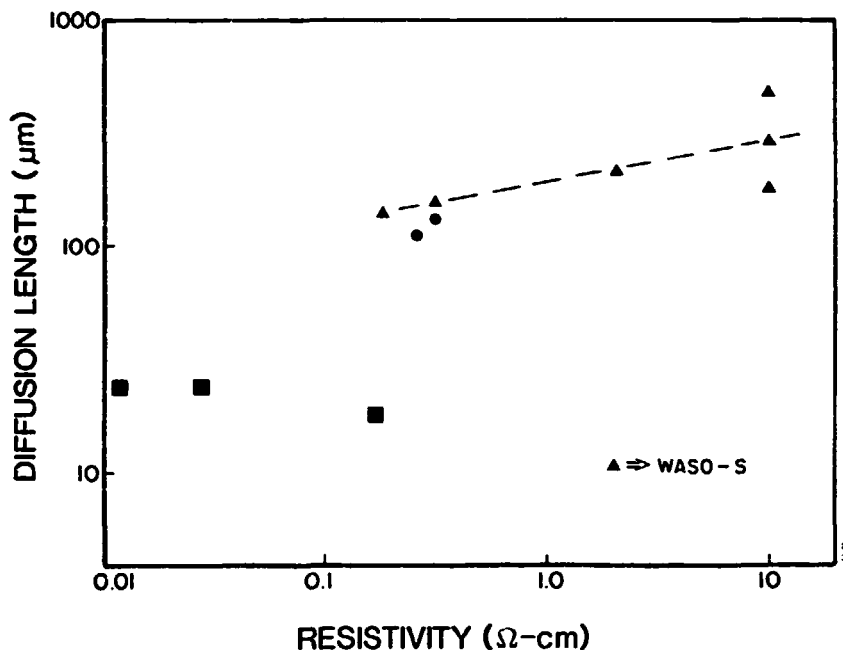


FIGURE 1. DIFFUSION LENGTH AS A FUNCTION OF RESISTIVITY. The dotted line indicates the functional dependence of  $L_D$  upon  $N_A$  that is assumed in our theoretical calculations.

TABLE I. CELL PERFORMANCE DATA FOR Si EVALUATION EXPERIMENT

GROUP	GRADE	RES. ( $\Omega\text{cm}$ )	$L_D$ ( $\mu\text{m}$ )	$V_{OC}$ (mV)	$J_{SC}$ (mA/cm $^2$ )	FF (%)	EFF (%)
A	CZ	0.17	18	585 (003)	18.5 (0.6)	77.7 (2.7)	8.4 (0.5)
B	FZ	0.26	109	598 (001)	22.3 (0.1)	79.0 (0.7)	10.5 (0.1)
C	WASO-S (FZ)	0.18	139	597 (002)	22.3 (0.1)	77.3 (1.4)	10.4 (0.2)
D	WASO-S (FZ)	0.33	154	599 (001)	22.8 (0.1)	78.2 (1.0)	10.7 (0.1)
E	WASO-S (FZ)	2.1	212	583 (001)	23.4 (0.1)	78.9 (0.3)	10.8 (0.1)
F	WASO-S (FZ)	10	462	571 (001)	24.4 (0.1)	77.4 (0.3)	10.8 (0.1)
G	WASO-S (FZ)	10	227	563 (004)	24.1 (0.2)	77.1 (0.4)	10.5 (0.2)
H	FZ	0.32	129	597 (001)	22.8 (0.1)	78.9 (0.5)	10.7 (0.1)
I	CZ	0.027	—	530 (036)	12.0 (0.1)	54.6 (16.8)	3.8 (0.7)
J	CZ	0.012	—	364 (079)	7.6 (.02)	53.2 (1.8)	1.5 (0.4)

NOTES: Area = 4 cm $^2$ , T = 28°C,  $L_D$  derived from quantum efficiency curves (9). Standard deviation shown in parenthesis.

Careful inspection of Table I indicates a large variation in fill factor (FF) for lower resistivities; this variation increases with decreasing resistivity. An examination of the dark I-V curves for representative cells, shown in Figure 2, indicates that leakage current increases as resistivity decreases. Through experimentation, we determined that this leakage current arises at the edges of the solar cells, which in our process are cut from the original wafers with a diamond wheel dicing saw. Etching of the edges to remove the saw damage removes this leakage path but also removes some active junction area. The deleterious effects on  $J_{SC}$  that edge etching causes can be minimized by either use of mesa etching defined by photolithography, or by using an ion implantation mask similarly defined so as to restrict the junction from kerf areas. Both methods were found to reduce the leakage current to negligible levels. For large-area cells in which edge leakage current is small compared to the diode forward current, this type of processing will probably be unnecessary.

ORIGINAL PAGE IS  
OF POOR QUALITY

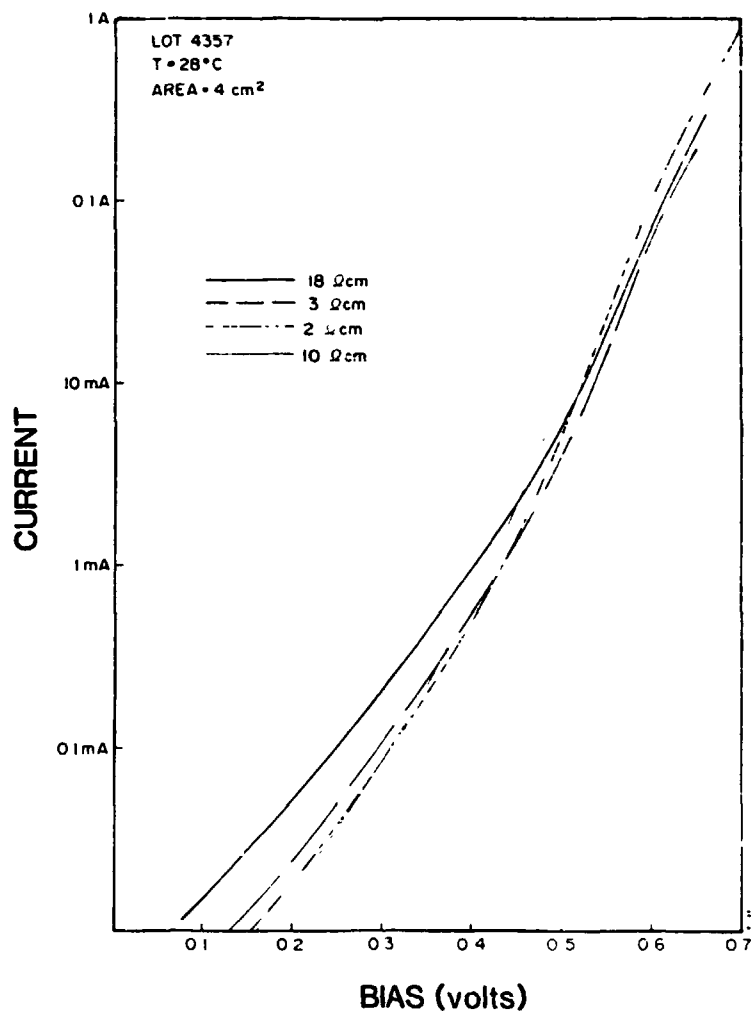


FIGURE 2. DARK I-V FOR REPRESENTATIVE CELLS OF VARIOUS RESISTIVITIES.

Figure 3 illustrates a comparison of measured external quantum efficiency (QE) data to the results of cell modelling, for a representative cell from group G in Table I. Good qualitative agreement is obtained. Exact fitting was not attempted for two reasons: first, the absolute error in the QE data is not precisely known and second, the code cannot model position dependent parameters that are believed to be important in the emitter. Integration of the model QE data, however, yields good agreement with measured  $J_{SC}$ , and this is shown as a function of resistivity in Figure 4 with front surface recombination velocity as a parameter. In Figure 5 we present a comparison of the measured  $V_{OC}$  data to the calculated values, with band gap narrowing ( $\Delta E_g$ ) as a parameter. The modelling suggests that for low resistivity Si, band gap narrowing and surface recombination velocity dominate  $V_{OC}$ .

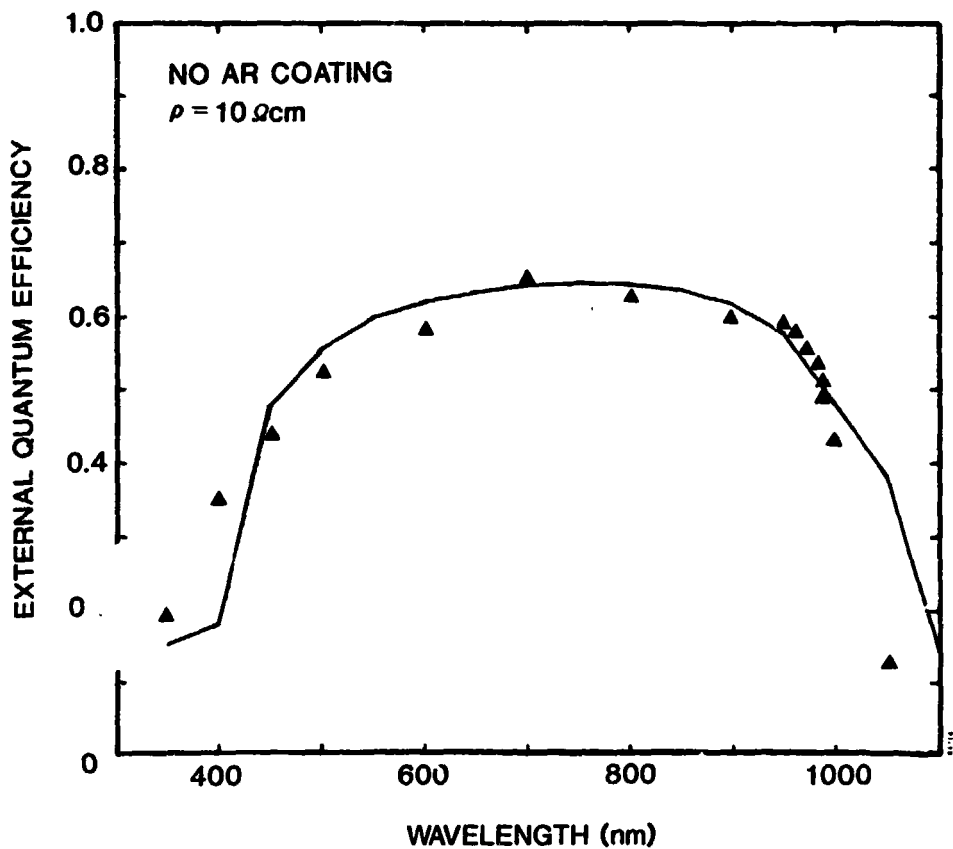


FIGURE 3. COMPARISON OF QUANTUM EFFICIENCY DATA TO MODEL CALCULATIONS FOR A CELL FROM GROUP G, TABLE I.

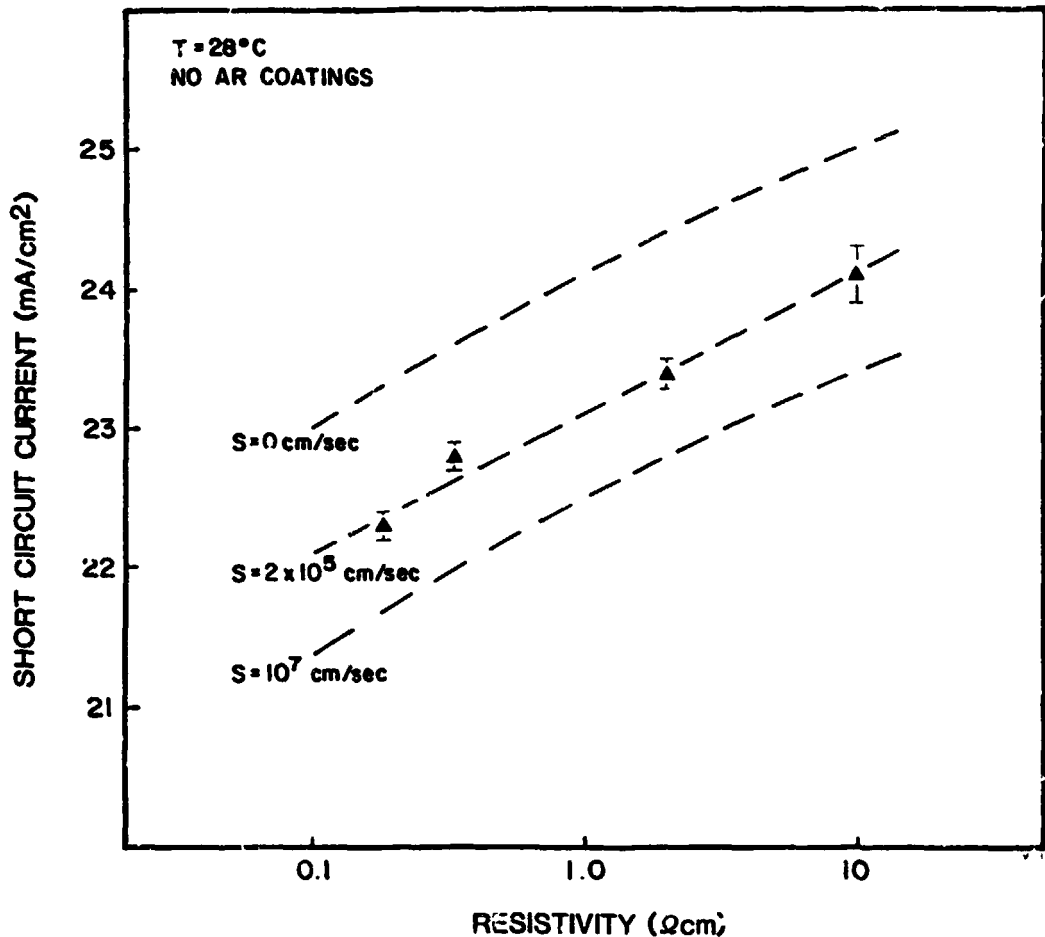


FIGURE 4. COMPARISON OF MEASURED AND CALCULATED  $J_{sc}$  AS A FUNCTION OF BASE ACCEPTOR CONCENTRATION.

We elected to work with cells of conventional thickness, even though calculations have shown that thin cells have theoretical advantages if minority carrier mirrors and light-trapping can be achieved (10). Our choice avoided the extraordinary care that handling thin ( $\sim 50 \mu\text{m}$ ) cells requires. The modelling of cells with conventional thickness ( $\sim 400 \mu\text{m}$ ) indicated that best efficiency would be obtained from low resistivity Si, provided that the emitter saturation current could be reduced, thus indicating the importance of pursuing research on emitter design.

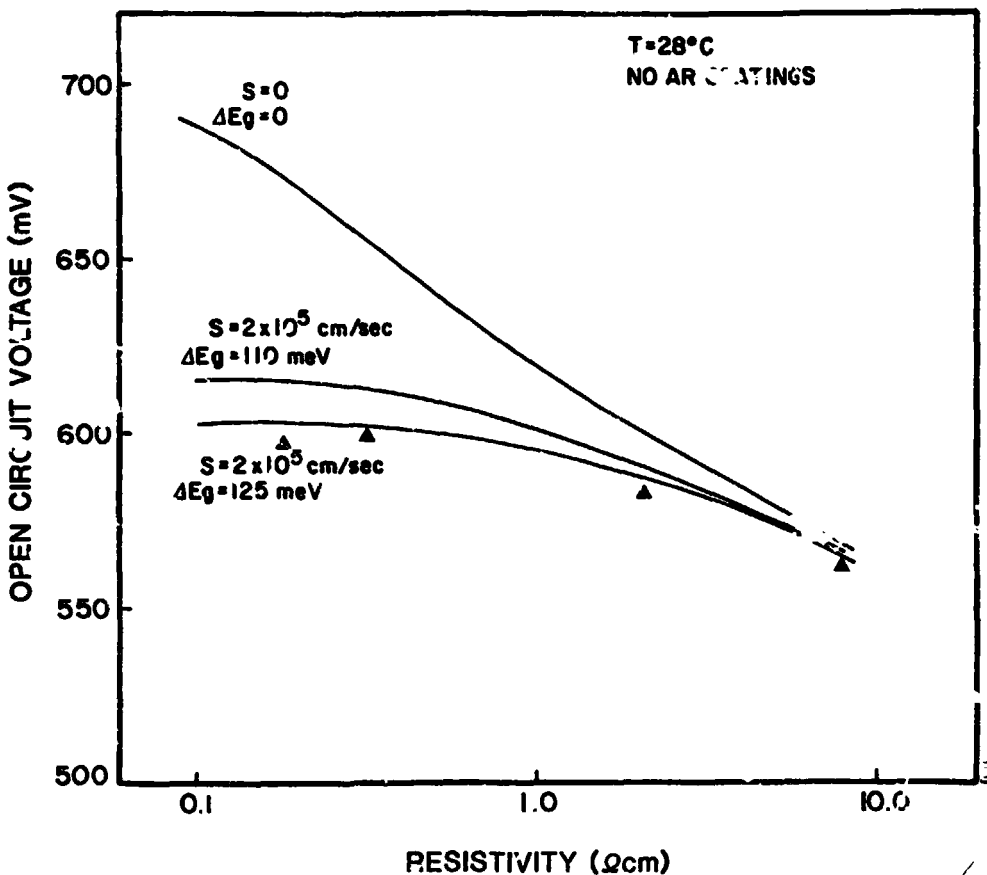


FIGURE 5. COMPARISON OF MEASURED  $V_{OC}$  DATA TO MODEL CALCULATIONS.

#### EMITTER EFFECTS

In a recent paper, we analyzed the importance of reduction of peak emitter dopant concentration, and it was shown that a very wide range of doping concentrations can be achieved with ion implantation (4). In Figure 6, we reproduce data that indicate that optimal QE at 350 nm is obtained for either arsenic or phosphorus emitter dopant concentrations of about  $2 \times 10^{19} \text{ cm}^{-3}$ .  $V_{OC}$  appears to have a peak in this range as well, as shown in Figure 7. Unfortunately, the actual emitter concentration for which the maximum  $V_{OC}$  is obtained is obscured by low base diffusion length; i.e. in the neighborhood of the optimal donor concentration, the  $V_{OC}$  is base-limited. We will return to this point in a later section.

Figures 6 and 7 indicate that there is an advantage to passivating the front surface when shallow ( $\sim 0.2 \mu\text{m}$ ) junctions are employed. Our experience indicates that as the junction is made deeper, the beneficial effects of passivation diminish; however, we have not conducted controlled experiments on this aspect.

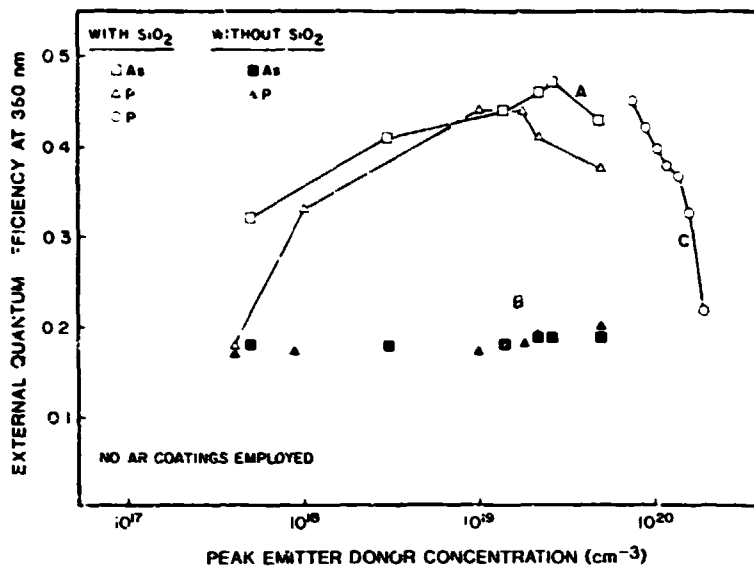


FIGURE 6. QUANTUM EFFICIENCY AT 350 nm. (A) Passivated As and P implanted emitters in 0.2 ohm-cm Si, (b) Non-passivated As and P implanted emitters in 0.2 ohm-cm Si, and (C) Passivated P implanted emitters in 0.3 ohm-cm Si.

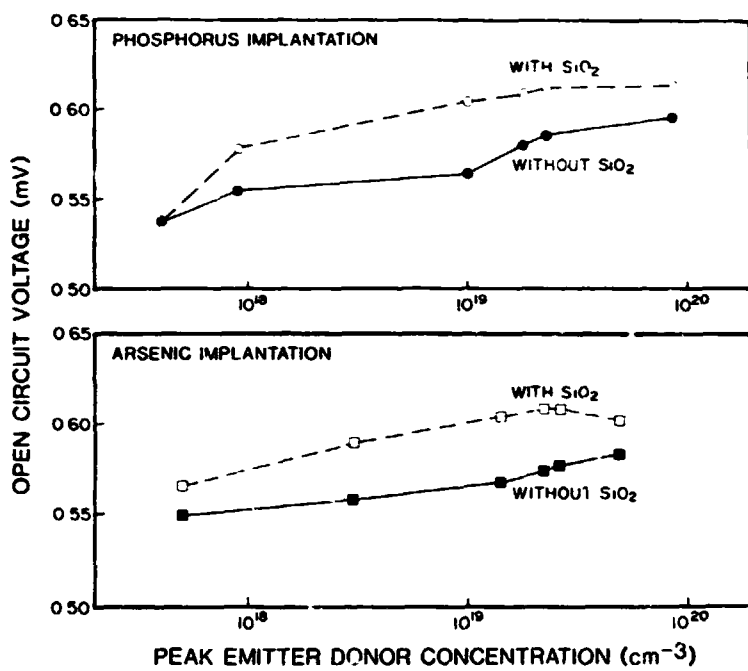


FIGURE 7.  $V_{oc}$  AS A FUNCTION OF  $N_D$ , WITH AND WITHOUT  $\text{SiO}_2$  PASSIVATION.

Surface preparation can often affect the attributes of the ion-implanted emitter. In a later section, we describe the use of texture-etching to reduce reflectivity and enhance absorption. This etching, however, increases the front surface area, which necessitates a change in the ion implantation dose. To identify the optimal ion implantation dose for such an etched surface, we fabricated texture-etched solar cells with a range of doses. Details of this experiment are reported in reference 2. Figure 8 replicates the  $V_{oc}$  data for cells having  $\text{SiO}_2$  passivation and for the same cells with  $\text{SiO}_2$  removed. It can be seen from Figure 8 that the removal of the  $\text{SiO}_2$  has a strong effect on  $V_{oc}$ .

There would seem to be three factors that control minority-carrier transport in the emitters of both the textured and polished devices: deleterious surface recombination, deleterious recombination and/or energy gap narrowing resulting from heavy doping effects, and advantageous minority-carrier reflection by the field resulting from the gradient of the doping. When  $\text{SiO}_2$  surface passivation is present, the optimal ion implantation dose is approximately  $5 \times 10^{15}$  ions/cm<sup>2</sup> for a textured surface. Use of higher doses would seem to introduce deleterious heavy doping effects in the emitter which cause an increase in the saturation current. The existence of enhanced recombination in the near surface region is suggested by spectral response measurements that show that blue response decreases as the doping is increased (Figure 6). For lighter implantation doses, a loss in minority-carrier reflection occurs, owing to the reduction in the gradient of the doping near the surface. This reduction in doping perhaps allows an increase in carrier recombination at the front contact, and so  $V_{oc}$  decreases as the concentration is decreased. For the case in which the  $\text{SiO}_2$  passivation is removed, the recombination at the surface exerts a strong influence on  $V_{oc}$ . In such a case, an increase in the peak dopant concentration that results from increase of dose increases the reflection of minority carriers, but the improvement is limited.

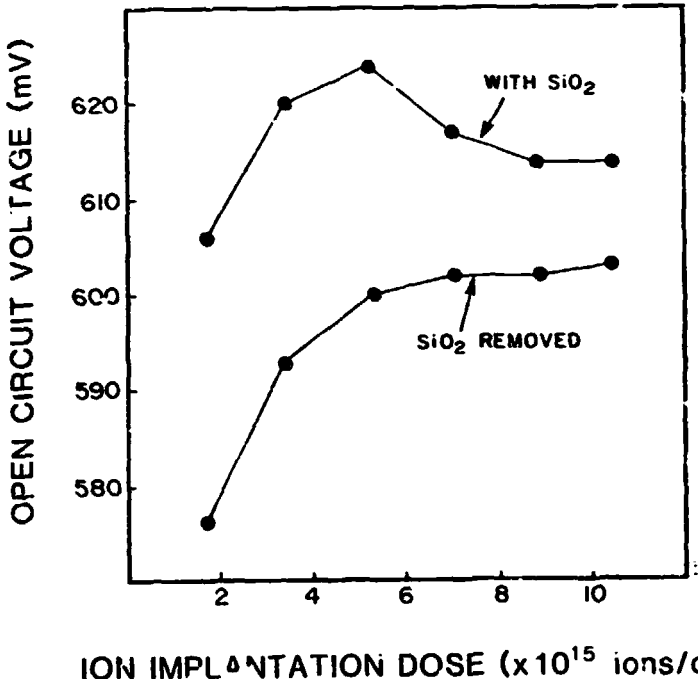


FIGURE 8. OPEN-CIRCUIT VOLTAGE AS A FUNCTION OF ION-IMPLANTATION DOSE FOR TEXTURE-ETCHED CELLS. The dose shown is the total dose measured by the implanter and is not corrected for the texture present on the target.

The optimization and theoretical analysis of our junction formation process applied to a textured surface requires knowledge of the resultant doping profile formed by the above implantation parameters on the {111} surfaces of the pyramids. For diffused junctions, one may perhaps assume that the junction profile replicates that which is formed on a standard {111} surface. It is not clear, however, that the depth distribution of implanted ions is equivalent to that obtained in an ordinary polished wafer, owing to scattering effects that may differ in the two cases. A further difference between diffusion and ion implantation is the increase in surface area mentioned above that obtains when texture is present. This increase requires a corresponding increase in ion dose.

For the above reasons, measurement of the dopant profile would be desirable. Unfortunately, the textured surface is not easily profiled using conventional techniques such as secondary ion mass spectroscopy, owing to obvious difficulties with depth calibration. For this reason, we conducted an experiment based upon ion implantation of a polished (111) wafer, suitably oriented with respect to the ion beam, to simulate the implantation of the {111} facets of the pyramids. This experiment is described in greater detail in reference 12.

A polished control (100) wafer was first implanted with  $^{31}\text{P}^+$  using the conventional geometry. The implantation energy was 5 keV and the dose was  $2.5 \times 10^{15}$  ions/cm<sup>2</sup>. An experimental (111) wafer was then implanted with  $^{31}\text{P}^+$  at 5 keV to a dose of  $5.2 \times 10^{15}$  ions/cm<sup>2</sup>, with the (111) surface oriented at an angle of 54.7° with respect to the ion beam to replicate the orientation of the facets of the textured surface. The specific dose, which includes an area correction related to the implantation angle, was  $3 \times 10^{15}$  ions/cm<sup>2</sup>. Both wafers were then annealed in flowing dry N<sub>2</sub> using a three step process: 550°C-2hr., 850°C-15 min., 550°C-2hr. with ramping between steps. Dry oxygen was admitted to the gas stream during the 850°C step to grow the thin oxide necessary for passivation.

Spreading resistance analysis was obtained for both wafers, and is shown in Figure 9. The analysis indicates that the profiles are without detectable difference. This is not surprising, since the implantation parameters for polished and textured wafers were separately optimized for high cell performance. The value of the peak dopant concentration obtained in this experiment has been used in the modelling which follows in the next section.

To further refine our solar cell emitters, we have been investigating the role of recombination at the front ohmic contact. To this end, we have been experimenting with the reduction of ohmic contact area, while keeping the shadow loss constant, as has been done elsewhere (13). Figure 10 illustrates two methods of implementing this technique. In method A, the opening in the passivating oxide through which contact is made is reduced in width so that the opening is more narrow than the grid line. In method B, the openings are small separate squares. Both techniques require photolithography and alignment; however, one method of producing type A contacts would be to make the grid lines as narrow as the desired openings in the oxide. The width of the lines might then be increased to the desired width by electroplating, thus obviating alignment.

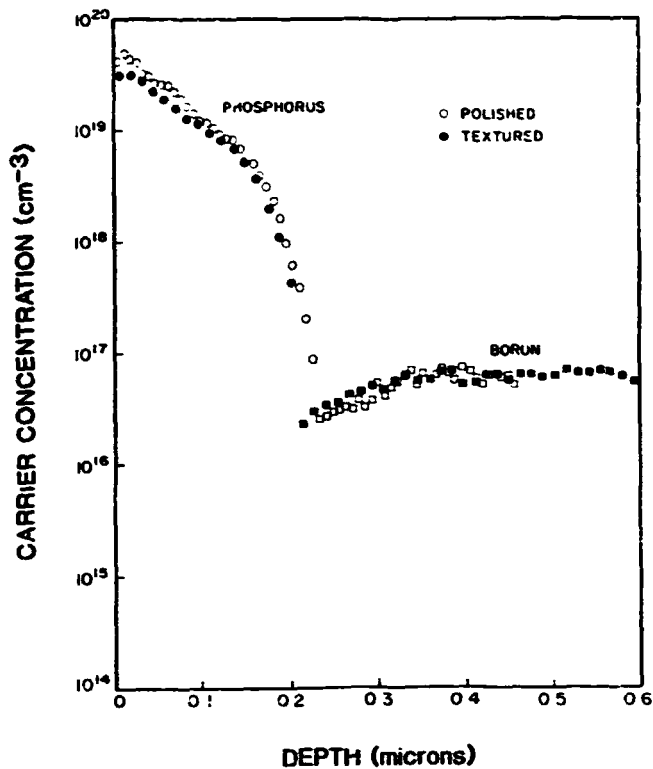


**FIGURE 9.** SPREADING RESISTANCE ANALYSIS OF A SIMULATED TEXTURED (111) WAFER AND A (100) CONTROL.

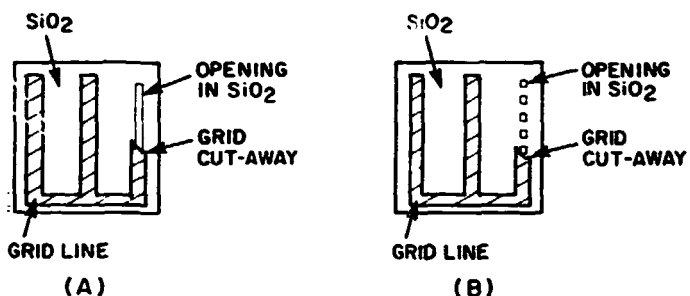


**FIGURE 10.** TWO METHODS OF REDUCING OHMIC CONTACT AREA.

Results with this type of processing are thus far inconclusive. In Figure 11 we replicate data from an experiment in which the ohmic contact area was varied as described above (4). Best results were achieved for reduced area, but the saturation current in these devices may arise mainly in the base, and so the optimal value of ohmic contact area may be obscured. Further experiments are in progress and will be reported at a later time.

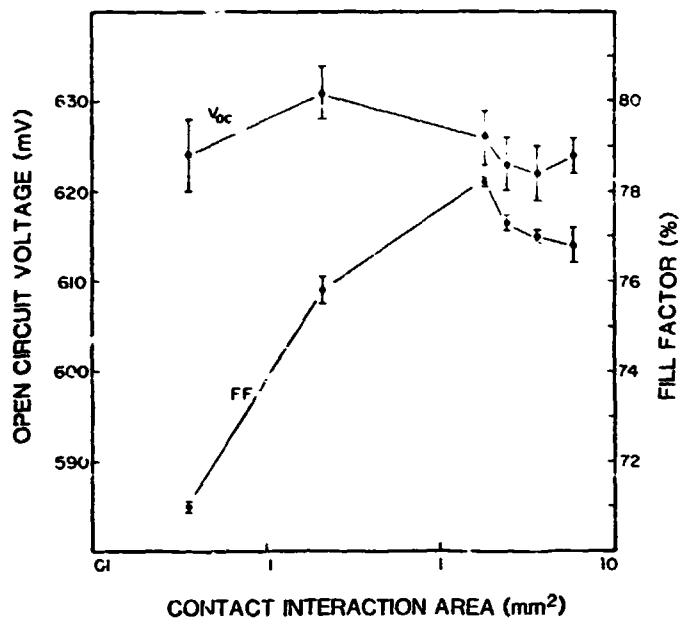


FIGURE 11.  $V_{\text{oc}}$  AND FF AS A FUNCTION OF OHMIC CONTACT AREA.  
(Base resistivity is 0.3 ohm-cm.)

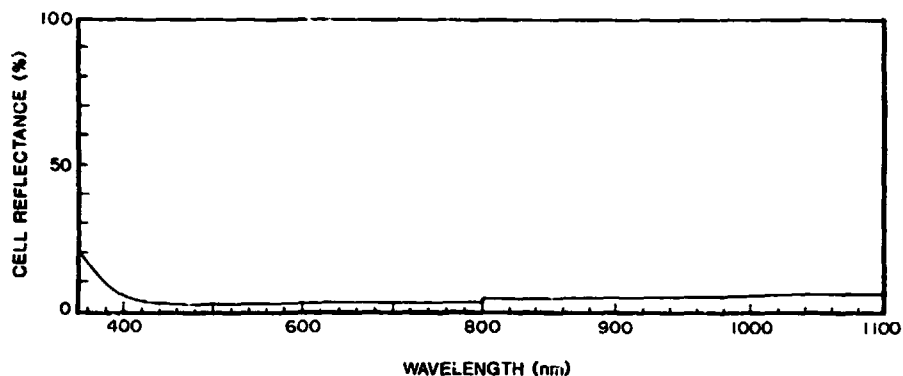


FIGURE 12. REFLECTION LOSS FOR A TEXTURED PASSIVATED SOLAR CELL.

Our results thus far on emitter design indicate the importance of both reduction of emitter dopant concentration and use of passivating oxide. This passivating oxide exerts a negligible influence on the reflection loss. To emphasize this point, we show in Figure 12 the measured reflectivity (courtesy of Dr. D. Arvizu, Sandia) from a textured solar cell. It can be seen that the reflection loss is indeed very small. The passivation can also be applied to sheet materials without severely affecting the AR coating. Recently we applied our emitter formation process to nonagon EFG ribbon. AM1 efficiency prior to AR coating was 9.7%. After evaporation of a single  $TiO_2$  layer, efficiency increased to 13.2%, indicating a gain of 36%; higher gain would be possible with a more suitable AR coating (such as  $Ta_2O_5$ ).

### HIGH EFFICIENCY CELL DESIGN

Figure 13 illustrates the details of the solar cell structure yielding the highest efficiency to date. The texture-etched front surface is ion-implanted to form the emitter, as discussed in the previous section. The surface is provided with a thin layer of  $SiO_2$  to reduce the front surface recombination velocity. An AR coating of  $Ta_2O_5$  is applied on top of the  $SiO_2$ ; the thickness of this layer is optimized to minimize the reflection resulting from the presence of the  $SiO_2$ . We have not reduced the ohmic contact area in this design.

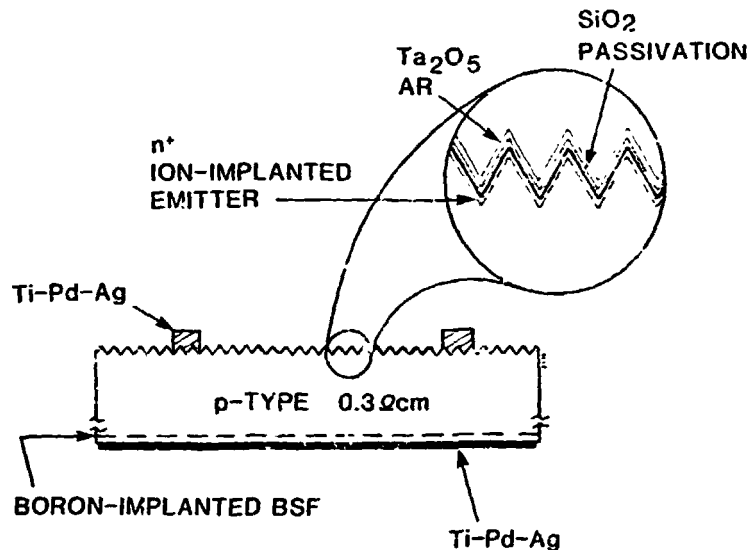


FIGURE 13. ILLUSTRATION OF THE SOLAR CELL STRUCTURE INVESTIGATED IN THIS WORK (not to scale).

Table 2 indicates the fabrication process for this cell design. The back surface is first implanted with  $^{11}\text{B}^+$  and annealed to form a  $\text{p}^+$  region. During the anneal, a thick surface oxide is grown to be used later for masking purposes. The resulting  $\text{p}^+$  layer is about 1  $\mu\text{m}$  deep and has a peak concentration of  $10^{20} \text{ cm}^{-3}$ (14). Because the diffusion length is much less than the cell thickness, the  $\text{p}-\text{p}^+$  junction is probably not effective as a back surface field (15); however, the  $\text{p}^+$  region does aid the formation of a low resistance back contact.

TABLE 2. CELL FABRICATION PROCESS

Implant back	$^{11}\text{B}^+ 50 \text{ keV}, \times 10^{15} \text{ ions/cm}^2$	
Anneal/oxide	$550^\circ\text{C} -- 2 \text{ hrs.}$	dry $\text{N}_2$
	$950^\circ\text{C} -- 2 \text{ hrs.}$	wet $\text{O}_2$
Pattern oxide	Acid etch	
Texture	Hydroxide etch	
Implant front	$^{31}\text{P}^+ 5 \text{ keV}, \text{ dose-variable}$	
Anneal/oxidize	$550^\circ\text{C} -- 2 \text{ hrs.}$	
	$850^\circ\text{C} -- 15 \text{ min.}$	
	$550^\circ\text{C} -- 2 \text{ hrs.}$	
Apply contacts	Evaporated Ti-Pd-Ag	
Saw to size	2 cm x 2 cm	
Plate contacts	Ag	
Apply AR coating	Evaporated $\text{Ta}_2\text{O}_5$	
Test	AM1, 100 mW/cm $^2$ , 28°C	

As discussed earlier, the surface oxide on the front was patterned to form an emitter ion implantation mask. The oxide mask defined the edges of the front phosphorus implant and so formed a planar emitter structure on each solar cell.

After patterning of the front oxide, the fronts of the wafers were texture-etched in a potassium hydroxide solution. Oxide on the back protected the boron implant from the etch. The fronts were then implanted with  $^{31}\text{P}^+$  and annealed as described in the previous section. Evaporated Ti-Pd-Ag contacts were applied to both sides of the wafers and were patterned on the fronts using the photolithographic lift-off process. Electroplating was used to decrease the contact line resistance. The final step consisted of electron-beam evaporation of a  $\text{Ta}_2\text{O}_5$  AR coating.

The resulting cells have been described in several recent publications (2, 16). Efficiency of up to 18% has been obtained, and the devices have been well characterized. We report here that an abbreviated form of the above process has been applied to Czochralski wafers supplied by Arco Solar Crystal Production. Efficiency of 16.8% was achieved (AMI, 28°C) and higher efficiency may be possible if the complete process is applied.

In Table 3, we summarize calculations of theoretical efficiency that indicate aspects of cell design that limit efficiency in the 18%-efficient FZ cells. The first entry in the table indicates the limit efficiency for a cell with width of 381  $\mu\text{m}$ , made from 0.3 ohm-cm silicon. The only loss mechanism included in this calculation is Auger recombination (17); perfect light trapping and minority carrier mirrors are assumed (10). It is interesting that the upper limit to  $J_{\text{SC}}$  is 43.8 mA/cm<sup>2</sup>, considerably higher than has been obtained in actual cells. Thus, considerable improvement is possible in  $J_{\text{SC}}$ . If neither light-trapping nor a back surface reflector (BSR) is present, the limit to  $J_{\text{SC}}$  is 42.2 mA/cm<sup>2</sup>. Incorporation of actual reflection loss measured on a high efficiency cell (see Figure 12) indicates that  $J_{\text{SC}}$  can be as high as 40.6 mA/cm<sup>2</sup>.

The diffusion length measured on our best cells is about 150  $\mu\text{m}$ . Replacement of the Auger-limited diffusion length ( $\sim 900 \mu\text{m}$ ) with the actual value reduces the  $J_{\text{SC}}$  to 36.9 mA/cm<sup>2</sup>. Thus, a considerable amount of current is lost in our cells owing to bulk recombination. This loss can be overcome by increasing the diffusion length through more careful processing or by gettering. An alternative would comprise thinning the cell and adding a BSR.

The  $V_{\text{OC}}$  indicated for a 150  $\mu\text{m}$  diffusion length is 649 mV. The calculation of  $V_{\text{OC}}$  is extremely sensitive to the value of the effective masses, or in another formalism, to the value of the intrinsic concentration assumed. In our calculation, we used Fermi statistics with an effective density of states given by the average effective masses for electrons and holes (18). Owing to uncertainties in the effective masses, the effective density of states, and to heavy-doping effects in general, this calculation can be considered only as a rough estimate of the  $V_{\text{OC}}$ .

Inclusion of front surface recombination and bandgap narrowing reduces  $V_{\text{OC}}$  to values as low as 618 mV, if the data from reference 11 is used. By using a value for  $\Delta E_g$  of 70 meV, we find good agreement with experiment. This may reflect the fact that our model assumes uniform doping, so 70 meV is perhaps an average value characterizing the heavily doped region near the surface and the lightly doped region beneath it. The shadow loss in our cells is approximately 3.5%; however, the reflection loss (already subtracted) includes reflection from the contact. Therefore, we only include a shadow loss of 2% in our calculation. Inclusion of the measured series resistance of 0.32 ohm-cm<sup>2</sup> (2) drops the FF to 81.6%. It can be seen that reasonable agreement with an experimental cell is attained.

The results in Table 3 reveal that a large amount of carriers are lost to bulk recombination. To quantify the effects of  $L_D$  on  $J_{\text{SC}}$ , we modelled the cell described above with  $L_D$  as a parameter. The result is shown in Figure 14. It can be seen that for the case of no BSR, increase in  $L_D$  to 200  $\mu\text{m}$  yields nearly 1 mA/cm<sup>2</sup> gain. The addition of a BSR with reflectivity of 90% would increase  $J_{\text{SC}}$  to 36.6 mA/cm<sup>2</sup>; increasing  $L_D$  to 200  $\mu\text{m}$  in that case would yield  $J_{\text{SC}}$  of over 37 mA/cm<sup>2</sup>. In the next section we will describe experiments intended to raise  $L_D$  to over 200  $\mu\text{m}$ .

**TABLE 3. ANALYSIS OF LOSS MECHANISMS OF SPIRE'S HIGH EFFICIENCY SOLAR CELLS**

	$V_{oc}$ (mV)	$J_{sc}$ (mA/cm <sup>2</sup> )	FF (%)	EFF (%)
Limit Efficiency of 0.3 Ωcm cell (Auger recomb. only)	713	43.8	84.7	26.5
No Light-Trapping	713	43.0	84.7	26.0
No BSR	712	42.2	84.7	25.5
Finite Reflection Loss	711	40.6	84.7	24.5
SRH Recombination ( $L_D=150\mu m$ )	649	36.9	83.6	20.0
Front Surface Recombination ( $S=2 \times 10^4$ cm/sec)	646	36.3	83.6	19.6
Bandgap Narrowing $\Delta E_g$				
(100 meV)	618	36.3	83.0	18.6
(80 meV)	629	36.3	83.2	19.0
70 meV	633	36.3	83.3	19.2
$J_{oe}$ Penalty for Front Texture	625	36.3	83.3	18.9
Shadow Loss (2%)	624	35.6	83.3	18.5
Series R (0.32 ohm-cm <sup>2</sup> )	624	35.6	81.6	18.1
Actual Data, Cell 22B	627	35.9	80.0	18.0

Notes: Calculations assume base width is 381 μm, T=28°C, Intensity = 100mW/cm<sup>2</sup>, AM1.

In the event that efforts to raise  $L_D$  beyond 200 μm fail, one can consider thinning the base of the cell. A calculation of  $J_{sc}$  as a function of base width is shown in Figure 15, for the case of back surface reflectivity of 90%. For a cell with base width of 200 μm, an increase in  $J_{sc}$  of about 0.5 mA/cm<sup>2</sup> is gained. If the cell is thinned and  $L_D$  is raised to 200 μm,  $J_{sc}$  of greater than 37 mA/cm<sup>2</sup> will be attained.

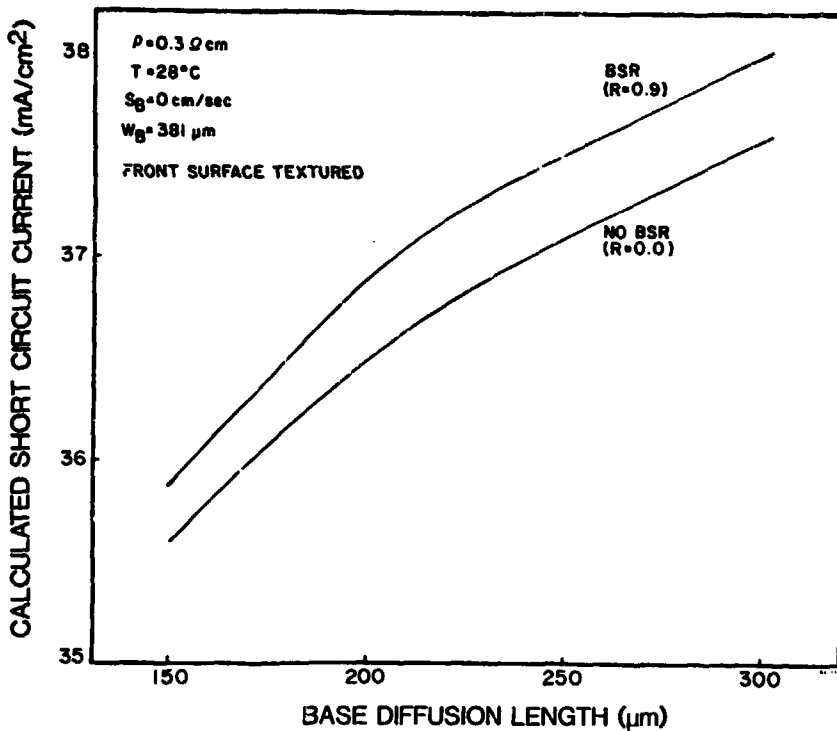


FIGURE 14. SHORT CIRCUIT CURRENT AS A FUNCTION OF DIFFUSION LENGTH.

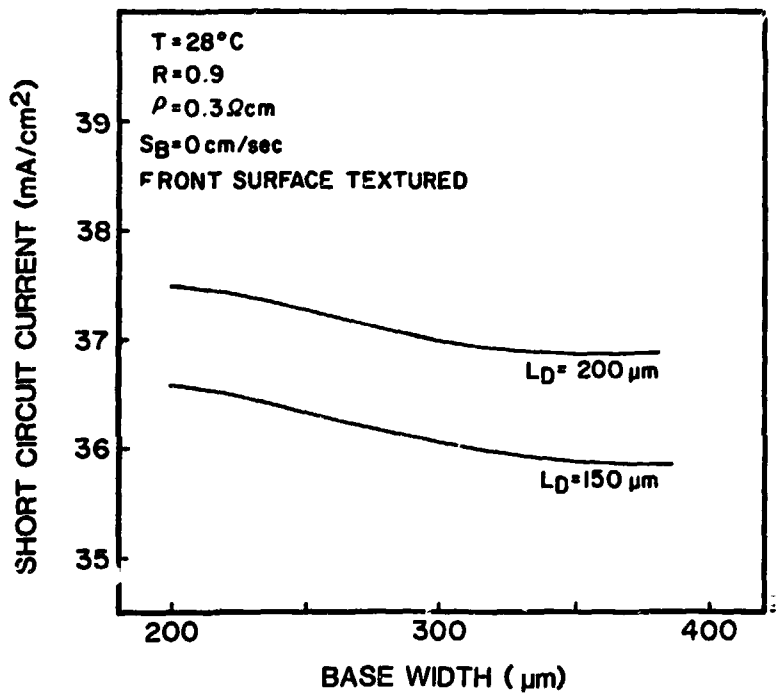


FIGURE 15. SHORT CIRCUIT CURRENT AS A FUNCTION OF CELL THICKNESS.

Improvements to  $L_D$  will also affect  $V_{OC}$ , although the gain is harder to quantify, owing to the large number of assumptions needed for calculation of  $V_{OC}$ . Nevertheless,  $V_{OC}$  as high as 660 mV is consistent with base resistivity of 0.3 ohm-cm and diffusion length of 200  $\mu$ m, and experiments to reduce the ohmic contact area may reduce the emitter saturation current to negligible levels, thus enabling us to realize the base-limited  $V_{OC}$ . Similar results have already been demonstrated elsewhere (3).

### EXPERIMENTS TO INCREASE $J_{SC}$

The preceding discussion has assumed that a BSR with reflectivity of 90% can be achieved. In fact we have developed such a BSR and in Figure 16 replicate experimental reflectance data from a polished AR-coated sample with Al evaporated on the back. The reflectivity of photons having energy less than the band gap, for which silicon is largely transparent, is greater than 90%. It is our assumption that the reflectivity of the BSR is as high for shorter wavelengths but the reflectance of photons with energy greater than the band gap has not been measured. However, the wavelengths that penetrate to the BSR are in general near the band edge, so the assumption is probably a good one.

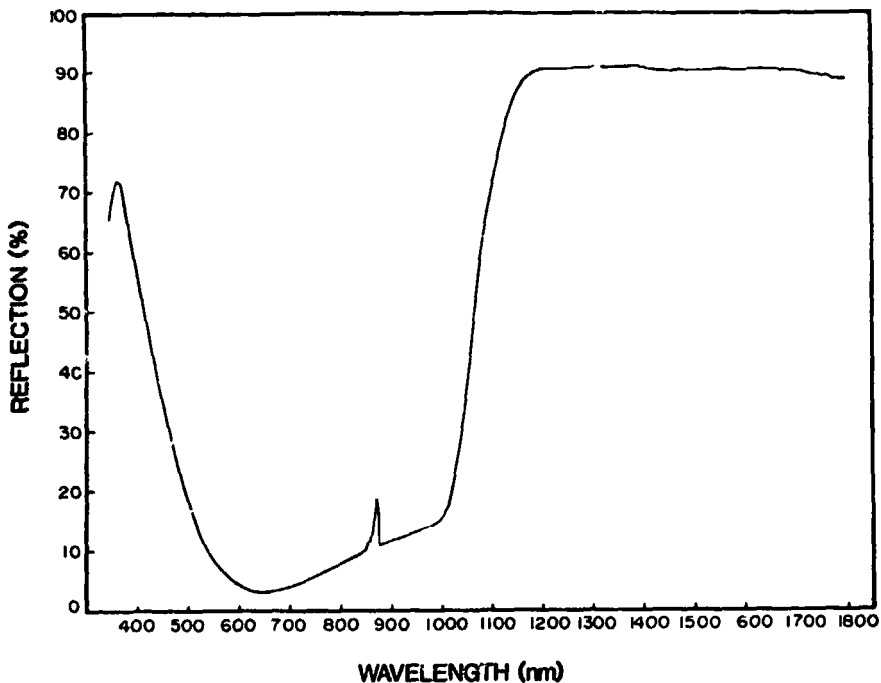


FIGURE 16. BSR REFLECTIVITY FOR AN AR-COATED CELL.

We have also examined the effect of our processing on cell lifetime. This was motivated by the anomalously low values of  $L_D$  that were obtained in a number of experiments, such as those reported in reference 4 and in earlier sections of this paper. In many of our emitter experiments, it was found that the base diffusion length had been degraded by the processing. We therefore devoted most of our attention to this problem. After a detailed examination of our furnace and gas lines, cleaning processes, annealing gases, and ramping, we identified our wet oxidation process to be a step that degrades lifetime. We have now eliminated wet oxidation from our sequence.

Recently we began experiments to increase diffusion length by gettering. The exact gettering processes that we are pursuing were taken from the literature and will be reported upon in a later publication. Owing to reservations about conducting an unusual process in our annealing tube, we used a sintering tube for the first gettering experiment. Since this tube is used for sintering solar cell contacts, it might be contaminated by Ti, Pd, or Ag. After a high temperature procedure in the sintering tube, the wafers were fabricated into cells. It was found that  $L_D$  in control cells had degraded to about 100  $\mu\text{m}$ , but  $L_D$  in the gettered cells increased to 170  $\mu\text{m}$ . It is our conjecture that annealing in a clean tube may yield much higher values of  $L_D$ , and this is presently being tested.

## CONCLUSIONS

Processing experiments have shown the importance of surface passivation, not only to  $V_{OC}$ , but also to  $J_{SC}$ . Analysis of loss mechanisms indicates that considerable improvement to  $J_{SC}$  may be obtained if diffusion length is increased. Improvement to  $V_{OC}$  is also possible by reducing emitter recombination. Many of these techniques can be applied with advantage to sheet materials. Certainly all of the above processing can be applied to CZ, with efficiency approaching that of FZ if gettering is successful in improving  $L_D$ . High efficiency can also be achieved with other sheet materials such as ribbon by using our junction formation and passivation techniques.

This work has indicated the manner in which the goal of 20% conversion efficiency may be achieved. Through process improvements such as gettering, thinning of the base, and addition of a BSR,  $J_{SC}$  of FZ cells may be increased to 38 mA/cm<sup>2</sup>. Improvements to the emitter, including reduction of ohmic contact area, may increase  $V_{OC}$  to 660 mV. We have already achieved FF of greater than 0.8. If these features can be integrated in one cell, efficiency of 20% will be achieved. The application of this processing to present-day sheet Si will be an important step toward the DOE goal of 15% efficiency at \$90/m<sup>2</sup>.

## ACKNOWLEDGMENTS

The authors are grateful to a number of contributors at Spire Corporation, and in particular acknowledge the assistance of H. Drake and L. Geoffroy with cell fabrication. The authors also wish to thank Dr. J. Milstein of SERI for help throughout this work. The authors thank Arco Solar Crystal Production and Mobil Solar Energy Corporation for supplying some of the materials used in this work. This research was supported by the U.S. Department of Energy through contracts with SERI, JPL and the DOE Small Business Innovative Research Office.

## REFERENCES

1. "Five Year Research Plan 1984-1988" of the U.S. Department of Energy National Photovoltaics Program Photovoltaic Energy Technology Division, Office of Solar Electric Technologies, U.S. DOE, (May 1983).
2. M.B. Spitzer, S.P. Tobin and C.J. Keavney, "High Efficiency Ion-Implanted Silicon Solar Cells," IEEE Trans. Electron Devices ED-31, No. 4 (1984).
3. M.A. Green, A.W. Blakers, J. Shi, E.M. Keller, and S.R. Wenham, "19.1% Efficient Silicon Solar Cell," Appl. Phys. Lett. 44, 1163 (1984).
4. M.B. Spitzer, C.J. Keavney, S.P. Tobin, F.A. Lindholm, and A. Neugroschel, "Mechanisms Limiting Open Circuit Voltage in Silicon Solar Cells," Record of the 17th IEEE Photovoltaic Specialists Conference, Orlando (1984).
5. M.B. Spitzer, "The Upper Limit to the Theoretical Efficiency of P-N Homojunction and Interfacial Layer Heterojunction Solar Cells," Ph.D. Thesis, Brown University (1981).
6. D. Redfield, "Multiple-pass thin-film silicon solar cell," Appl. Phys. Lett. 25, 647 (1974).
7. M. Wolf, "Updating the Limit Efficiency of Silicon Solar Cells," IEEE Trans. Electron Devices ED-27, 751 (1980); see also; D.L. Bowler and M. Wolf "Interactions of Efficiency and Material Requirements for Terrestrial Silicon Solar Cells," IEEE Trans. Components, Hybrids, and Manufacturing Technology, CHMT-3, 464 (1980).
8. M.B. Spitzer, "Basic Understanding of High Efficiency in Silicon Solar Cells," Annual Report for SERI Contract 2B-3-02090-3 (1984).
9. E.D. Stokes and T.L. Chu, "Diffusion Length in Silicon Solar Cells from Short-Circuit Current Measurements," Appl. Phys. Lett. 30, 425 (1977).
10. M. Spitzer, J. Shewchuk, E.S. Yera and J.J. Loferski, "Ultra High Efficiency Thin Silicon P.N. Junction Solar Cells Using Reflecting Surfaces," Rec. of the 14th IEEE Photovoltaic Specialists Conference, San Diego, 1980, p. 375.
11. W. Slotboom and H.C. de Graaff, "Measurements of Bandgap Narrowing in Si Bipolar Transistors," Solid-State Electronics 19, 857 (1976).
12. C.J. Keavney and M.B. Spitzer, "Solar Cell Junction Profiles in Ion-Implanted Texture-etched Surfaces," accepted for publication in J. Appl. Phys. (1984).
13. A Meulenberg and R.A. Arndt, "Surface Effects in High Voltage Silicon Solar Cells," Rec of the 16th IEEE Photovoltaics Specialists Conference (1982) p. 348.

14. M.B. Spitzer, M.M. Sanfacon, and R.L. Wolfson, "Ion Implanted Junctions for Silicon Space Solar Cells," Rec. of the 18th Intersociety Energy Conversion Engineering Conference, Orlando, 1983, p. 1213.
15. H.T. Weaver, "Ineffectiveness of Low-High Junctions in Optimized Solar Cell Designs," Solar Cells, 5, 275 (1982).
16. M.B. Spitzer, C.J. Keavney, S.P. Tobin, and J.B. Milstein, "Ion Implanted Cells with 18% Conversion Efficiency," Record of the 17th IEEE Photovoltaic Specialists Conference, Orlando (1984).
17. J. Dziewior and W. Schmid, "Auger coefficients for highly doped and highly excited silicon," Appl. Phys. Lett. 31, 346 (1977).
18. S.M. Sze, Physics of Semiconductor Devices, John Wiley & Sons, 1981.

## DISCUSSION

CISZEK: Mark, do you have any thoughts on how you might be able to get reduced area contact to a wafer through an oxide?

SPITZER: I'll have to draw a slide of that. What's the Green secret? I don't have to draw that, I can explain it. What you do is you make a very fine-line grid. It would not be suitable for carrying the currents that you want, but it has the area of the opening in the oxide that I showed. And then you overplay it, you let the electroplating balloon the grid lines in their proper proportions; then you are left with grid lines that just touch a very small area along the surface. There is no alignment involved. The problem with that, I think, is the grid lines fall off; you have to be careful. I don't like it.

QUESTION: You can cross the lines, you make your slot and then cross your grid lines, you'll get a dot contact.

SPITZER: I was worried in doing that technique. I was worried about depositing the AR and having stripes on the wafer.

QUESTION: Mark, in your 18% efficient cell the surface dopant concentration was  $3 \times 10^{18}$ , or what?

SPITZER: In the 18% cell we think it was  $3 \times 10^{19}$ . So we used the same implant parameters for that experiment, where we measured the profile, as had been used on the 18% cells.

OLSON: Both in your work and Ajeet's you applied some of the things you learned to sheet materials, and I really think with some neat results. I think one interesting point to make is that your work on the good float-zone material is really a leading edge, and I think it is really important to have the high-efficiency work on this high-quality material lead the way. And it's clear that now you are beginning to apply it to work on low-cost sheet material.

SPITZER: I agree with that. And there is one other thing that we are working on, and that is to scale up the area of the cell. I think it also has to be applied to a fairly large-area device.

OLSON: It's there we are going to really learn what's really limiting the performance, and ultimately that might pay off.

SPITZER: I agree. I think we should stay with float-zone for a while.

JOHNSON: Mark, what was the sheet resistance of your emitter?

SPITZER: The baseline emitter that we started out was about 80 ohms per square and the one that is  $3 \times 10^{19}$  is about 200 ohms per square.

DAUD: Mark, could you tell me what the resistivity of the Czochralski silicon was that you got from ARCO?

**SPITZER:** Actually, I know what it is, but I don't have permission to disclose anything about the material, so you can ask one of the ARCO guys. But there is nothing crazy about it, its just ordinary stuff.